Faraday Discussions

RSC Publishing

Cite this: *Faraday Discuss.*, 2013, **163**, 95

PAPER

View Article Online
View Journal | View Issue

Probing ultrafast dynamics in photoexcited pyrrole: timescales for $^1\pi\sigma^*$ mediated H-atom elimination†

Gareth M. Roberts,[a] Craig A. Williams,[a] Hui Yu,[b] Adam S. Chatterley,[ac] Jamie D. Young,[a] Susanne Ullrich[b] and Vasilios G. Stavros*[a]

Received 5th December 2012, Accepted 7th January 2013
DOI: 10.1039/c2fd20140b

The heteroaromatic ultraviolet chromophore pyrrole is found as a subunit in a number of important biomolecules: it is present in heme, the non-protein component of hemoglobin, and in the amino acid tryptophan. To date there have been several experimental studies, in both the time- and frequency-domains, which have interrogated the excited state dynamics of pyrrole. In this work, we specifically aim to unravel any differences in the H-atom elimination dynamics from pyrrole across an excitation wavelength range of 250–200 nm, which encompasses: (*i*) direct excitation to the (formally electric dipole forbidden) $1^1\pi\sigma^*$ ($^1A_2$) state; and (*ii*) initial photoexcitation to the higher energy $^1\pi\pi^*$ ($^1B_2$) state. This is achieved by using a combination of ultrafast time-resolved ion yield and time-resolved velocity map ion imaging techniques in the gas phase. Following direct excitation to $1^1\pi\sigma^*$ ($^1A_2$) at 250 nm, we observe a single time-constant of 126 ± 28 fs for N–H bond fission. We assign this to tunnelling out of the quasi-bound 3s Rydberg component of the $1^1\pi\sigma^*$ ($^1A_2$) surface in the vertical Franck–Condon region, followed by non-adiabatic coupling through a $1^1\pi\sigma^*/S_0$ conical intersection to yield pyrrolyl radicals in their electronic ground state ($C_4H_4N(\tilde{X})$) together with H-atoms. At 238 nm, direct excitation to, and N–H dissociation along, the $1^1\pi\sigma^*$ ($^1A_2$) surface is observed to occur with a time-constant of 46 ± 22 fs. Upon initial population of the $^1\pi\pi^*$ ($^1B_2$) state at 200 nm, a rapid $^1\pi\pi^*$ ($^1B_2$) → $1^1\pi\sigma^*$ ($^1A_2$) → N–H fission process takes place within 52 ± 12 fs. In addition to ultrafast N–H bond cleavage at 200 nm, we also observe the onset of statistical unimolecular H-atom elimination from vibrationally hot S_0 ground state species, formed after the relaxation of excited electronic states, with a time-constant of 1.0 ± 0.4 ns. Analogous measurements on pyrrole-d_1 reveal that these statistical H-atoms are released only through C–H bond cleavage.

[a]*Department of Chemistry, University of Warwick, Library Road, Coventry, CV4 7AL, UK. E-mail: v.stavros@warwick.ac.uk*

[b]*Department of Physics and Astronomy, University of Georgia, Athens, GA 30602, USA*

[c]*Department of Chemistry, Durham University, South Road, Durham, DH1 3LE, UK*

† Electronic supplementary information (ESI) available. See DOI: 10.1039/c2fd20140b

1 Introduction

The gas phase spectroscopy and dynamics of heteroaromatic subunits of biomolecules have received considerable interest in the recent literature.[1–3] Notable examples include studies on DNA nucleobases[4–9] and aromatic amino acid chromophores[10–17] following the absorption of ultraviolet (UV) radiation. Whilst these studies lack the realistic environment to which these molecules ultimately function in—for example, surrounding solvent molecules or the hydrophobic cavity of an extended protein—such a 'bottom-up' approach has nonetheless enabled considerable insight into many of the key aspects of their photochemistry and photophysics. Recent work has indeed begun to demonstrate that these gas phase studies can be used as a benchmark for understanding how this behaviour may evolve in the condensed phase.[18–21]

In this discussion paper, we focus on the excited state photochemistry of pyrrole (molecular structure shown in inset in Fig. 1(a)). A five-membered aromatic heterocycle, pyrrole appears in a number of naturally occurring biomolecules—most notably it is present in heme, the non-protein component of hemoglobin, and as a subunit within the amino acid tryptophan. The prevalence

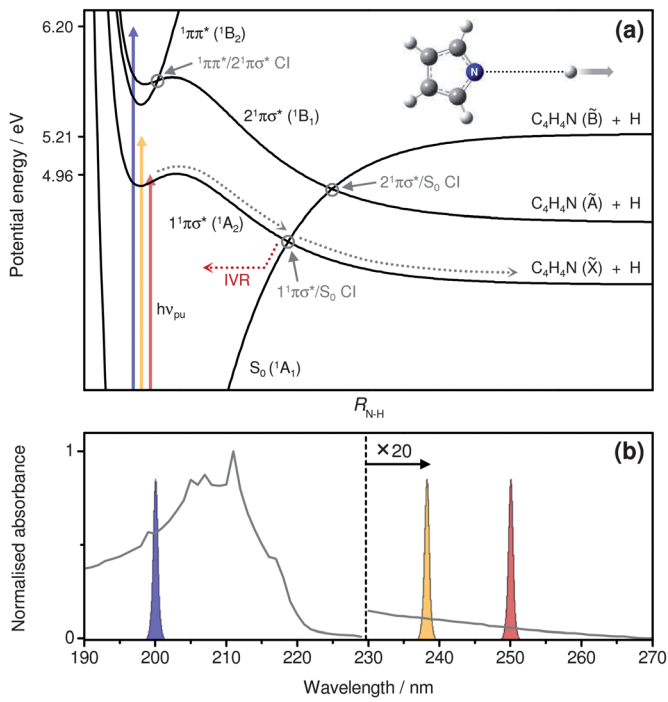

Fig. 1 (a) Schematic 1-D potential energy cuts of the S_0 ($^1A_1$), $1^1\pi\sigma^*$ ($^1A_2$), $^1\pi\pi^*$ ($^1B_2$) and $2^1\pi\sigma^*$ ($^1B_1$) electronic states of pyrrole (molecular structure inset), as a function of N–H bond length (R_{N-H}). Excitations ($h\nu_{pu}$) at pump wavelengths of 250 (red), 238 (yellow) and 200 nm (blue) are represented by vertical arrows. Conical intersections (CIs) along the R_{N-H} coordinate are labelled in grey, while intramolecular vibrational energy redistribution (IVR) after coupling back on to S_0 is represented by the dotted red line. (b) Vapour phase UV absorption spectrum of pyrrole between 270–190 nm (grey). Approximate spectral profiles of the fs pump pulses at 250 (red), 238 (yellow) and 200 nm (blue) are also shown.

of pyrrole in nature has triggered numerous spectroscopic studies, in both the time-[22,23] and frequency-domains,[24–28] as well as a number of theoretical investigations,[1,29–33] all aimed at unravelling the excited state dynamics which ensue after photoexcitation with UV radiation.

The UV absorption spectrum of pyrrole is shown in Fig. 1(b). Over past decades, there have been a number of theoretical studies conducted in an attempt to characterise the intense peak centred at ~210 nm.[34–39] Although the precise ordering of the electronic excited states in pyrrole still remains controversial, it is generally accepted that the majority of absorbance in this band arises from a $^1\pi\pi^*$ ($^1B_2$) ← S_0 ($^1A_1$) transition[26,29,39] (~15% has also been attributed to a $^1\pi\pi^*$ ($^1A_1$) ← S_0 ($^1A_1$) transition,[26,39] not shown in Fig. 1(a)). The pronounced resonances superimposed on top of this broad feature have been attributed to excitation to Rydberg states, with the strongest resonance at ~211 nm assigned by Roos *et al.*[39] to the origin band of the $^1\pi 3p_y$ ($^1B_1$) ← S_0 ($^1A_1$) transition. This broad absorption feature decreases significantly in intensity by ~220 nm, although a very weak tail of absorbance persists down to ~270 nm. This weak tail in the absorption spectrum has been assigned to at least three "optically forbidden" excited electronic states,[27] the most significant of which is the $1^1\pi\sigma^*$ ($^1A_2$) ← S_0 ($^1A_1$) transition. In the vertical Franck–Condon region this $1^1\pi\sigma^*$ ($^1A_2$) state possesses notable 3s Rydberg character associated with the N atom.[1,39] Although formally electric dipole forbidden in C_{2v} symmetry, excitation to $1^1\pi\sigma^*$ ($^1A_2$) can be vibronically induced *via* intensity borrowing from higher lying electronic states, *e.g.* $^1\pi\pi^*$ ($^1B_2$).[23,25–28]

In recent years there has been considerable interest in H-atom elimination dynamics from the N–H bond in pyrrole, mediated by the $1^1\pi\sigma^*$ ($^1A_2$) state.[22–28] This has largely been driven by the seminal theoretical work by Domcke, Sobolewski and co-workers.[1] These authors proposed that the highly efficient ultrafast relaxation dynamics of heteroaromatic molecules can be due, in part, to dissociative $^1\pi\sigma^*$ states localised along X–H (where X = N or O) bond coordinates. With specific reference to pyrrole and the corresponding schematic 1-D potential energy cuts (PECs) shown along its N–H bond coordinate (R_{N-H}) in Fig. 1(a), population directly imparted to the dissociative $1^1\pi\sigma^*$ ($^1A_2$) surface may evolve towards a $1^1\pi\sigma^*/S_0$ conical intersection (CI) and undergo non-adiabatic coupling. This can lead to either repopulation of the electronic ground state, S_0, or direct N–H bond cleavage to yield H-atoms with large amounts of kinetic energy (KE) and pyrrolyl radical co-fragments in their electronic ground state, $C_4H_4N(\tilde{X})$. Alternatively, when excitation occurs at higher photon energies, internal conversion (IC) from the strongly absorbing $^1\pi\pi^*$ ($^1B_2$) state can lead to subsequent population of the $1^1\pi\sigma^*$ ($^1A_2$) surface, also giving rise to rapid N–H bond scission or repopulation of S_0.[24,26–28]

Experimental determination of the exact branching ratio of population bifurcating into S_0 and radical photoproducts at the $1^1\pi\sigma^*/S_0$ CI is non-trivial.[40] However, one is able to measure the KE of the H-atoms eliminated following photoexcitation and then correlate features in the KE spectrum to H-atoms eliminated along the $1^1\pi\sigma^*$ ($^1A_2$) state, providing a signature for the participation of this state in the excited state dynamics;[24–28] ref. 3 provides a more general discussion on this approach to studying $^1\pi\sigma^*$ mediated dynamics in heteroaromatic molecules. For pyrrole, this was first demonstrated using photofragment translational spectroscopy (PTS) techniques by Blank *et al.*[24] upon excitation

at 193 and 248 nm, and later with velocity map ion imaging (VMI) techniques by Wei *et al.*,[25,26] following excitation at 217 and 243.1 nm. In the latter studies, H-atoms with high KE ($\sim$7500 cm^{-1}) were attributed to direct dissociation mediated by the $1^1\pi\sigma^*$ ($^1A_2$) state, whilst H-atoms with low KE were attributed to unimolecular dissociation from the S_0 ground state. Based on the measured KE of the H-atoms eliminated, the persistence of high KE D-atoms observed following deuteration of the N–H coordinate (pyrrole-d_1), and the near-limiting recoil anisotropy parameter ($\beta_2 = -0.95$), Wei *et al.* concluded that at 217 nm a $^1\pi\pi^*$ ($^1B_2$) $\rightarrow$ $1^1\pi\sigma^*$ ($^1A_2$) $\rightarrow$ N–H fission pathway occurred in <300 fs.[26] The wavelength range for studying this behaviour was extended in H(Rydberg) atom PTS (HRA-PTS) measurements by Cronin *et al.*[27] from $193.3 < \lambda < 254.0$ nm, enabling these authors to identify the onset for the $^1\pi\pi^*$ ($^1B_2$) state absorption channel ($\sim$218 nm) and also determine the N–H bond strength to be D_0(N–H) = 32850 $\pm$ 40 cm^{-1}. At wavelengths greater than 254 nm, no significant H-atom signal was observed by these authors.[27]

The first ultrafast time-resolved measurements of H-atom elimination from pyrrole (and indeed, any aromatic heterocycle) were reported in the seminal paper by Lippert *et al.*[22] In this work, the $1^1\pi\sigma^*$ ($^1A_2$) state was directly photoexcited at 250 nm and the H-atoms were probed as a function of pump–probe time delay through 2+1 resonance enhanced multiphoton ionisation (REMPI). The measured H^+ signal, as a function of increasing pump–probe delay, exhibited a bi-exponential rise profile, to which kinetic fits returned two time-constants, τ_1 and τ_2, with values of 110 $\pm$ 80 fs and 1.1 $\pm$ 0.5 ps, respectively.[22] Once again, with reference to the PECs along R_{N-H} in Fig. 1(a), τ_1 (110 fs) was attributed to the timescale for direct $1^1\pi\sigma^*$ ($^1A_2$) mediated N–H bond fission, proceeding *via* non-adiabatic passage through the $1^1\pi\sigma^*/S_0$ CI, yielding H-atoms with large amounts of KE in coincidence with $C_4H_4N(\tilde{X})$ radical co-fragments. The second, slower time constant, τ_2 (1.1 ps), was attributed to statistical unimolecular H-atom elimination from the hot S_0 ground state of pyrrole, following IC back onto S_0 at the $1^1\pi\sigma^*/S_0$ CI.[22] Most recently, Montero *et al.*[23] have performed ultrafast time-resolved ion yield (TR-IY) measurements on the pyrrole cation signal (pyrrole$^+$) to study the lifetimes of the initial photoexcited states of pyrrole at a number of wavelengths. From these studies, they infer a timescale of 15 $\pm$ 3 fs for the initially prepared wavepacket on the $1^1\pi\sigma^*$ ($^1A_2$) surface to evolve out of the vertical ionisation window, while at higher photon energies they report a timescale of 19 $\pm$ 3 fs for the $^1\pi\pi^*$ ($^1B_2$) $\rightarrow$ $1^1\pi\sigma^*$ ($^1A_2$) IC process to occur.[23] The dynamical picture arising from these combined experimental studies, in both the time- and frequency-domains, is also qualitatively supported by a number of *ab initio* studies, which include mixed quantum-classical trajectory[30–33] and fully quantum mechanical wavepacket calculations.[29]

To establish the timescales for H-atom elimination dynamics in pyrrole, we probe dissociated H-atoms using a combination of ultrafast TR-IY and time-resolved velocity map ion imaging (TR-VMI) following excitation at a number of wavelengths (250, 238 and 200 nm). The ability to obtain both energy *and* time information using TR-VMI enables us to determine the timescales for direct dissociation following excitation to the $1^1\pi\sigma^*$ ($^1A_2$) state and infer a timeframe for $^1\pi\pi^*$ ($^1B_2$) $\rightarrow$ $1^1\pi\sigma^*$ ($^1A_2$) coupling. Complementary TR-IY and TR-VMI measurements of D-atom elimination from pyrrole-d_1 (which is selectively deuterated at the N–H site), also enable us to: (*i*) investigate the role of both

statistical unimolecular N–H *and* C–H bond fission from pyrrole molecules in a vibrationally hot S_0 ground state, depending on the initially prepared excited state ($1^1\pi\sigma^*$ ($^1A_2$) or $^1\pi\pi^*$ ($^1B_2$)); and (*ii*) reveal the presence of tunnelling through a small exit barrier in the $1^1\pi\sigma^*$ ($^1A_2$) surface, prior to rapid N–H bond fission.

2 Experimental methods

The reader is directed to previous work for further experimental details of the TR-VMI apparatus[41,42] and therefore only a brief overview is provided here. TR-VMI experiments utilise femtosecond (fs) laser pulses derived from a commercial Ti:Sapphire oscillator and regenerative amplifier system (Spectra-Physics, Tsunami and Spitfire XP, respectively). The regenerative amplifier is set at 125 Hz for these experiments, delivering 3 mJ/pulse centred at 800 nm with a temporal full width at half maximum (FWHM) of ~40 fs. The fundamental output is subsequently split into three beams of equal energy. Of these three beams, one is up-converted into a 200 nm pump beam, which is achieved *via* frequency doubling the fundamental in a type-I β-barium borate (BBO) crystal to generate 400 nm, followed by successive frequency mixing (type-II and type-I BBO crystals, respectively) with the residual 800 nm pulses to generate third harmonic (267 nm) and finally the desired 200 nm fourth harmonic (~1 μJ/pulse). The remaining two beams are used to pump two optical parametric amplifiers (Light Conversion, TOPAS-C). One of these produces a tunable pump in the range 238–250 nm (3–4 μJ/pulse) whilst the second is used to generate the probe, set at 243.1 nm (~7 μJ/pulse) to selectively ionise any H-atoms *via* a 2+1 REMPI process, resonant with the two-photon allowed 2s ← 1s transition. The time-delay between pump and probe pulses (Δt) is controlled by passing the 800 nm seed beam for pump generation through a protected-gold hollow retroreflector mounted on a computer controlled delay stage (Physik-Instrumente, M-521.DD). The pump and probe pulses are focused through $f = 50$ cm MgF_2 and CaF_2 lenses, respectively, and recombined prior to entering the interaction region of a VMI spectrometer[43] where they perpendicularly intersect a molecular beam pulse seeded with pyrrole. The power densities of the pump and probe pulses are ~10^{11}–10^{12} and ~10^{13} W cm^{-2}, respectively. Non-resonant multiphoton ionisation of methanol is employed as a method for determining both the delay position corresponding to the temporal overlap of the pump and probe ($\Delta t = 0$), to within an accuracy of ±15 fs, and the associated cross-correlation/instrument response function (IRF). For these experiments a Gaussian IRF is measured with a FWHM of ~120 fs for pump wavelengths in the range 250–238 nm and ~160 fs for the 200 nm pump. The polarisation of both beams is set parallel to the plane of the imaging detector.

Molecular beam pulses are generated by seeding pyrrole (Sigma-Aldrich, >98%) molecules in helium (~2 bar) which are transferred into vacuum using an Even-Lavie pulsed solenoid valve[44] operating at 125 Hz, which is synchronized to the laser system. The valve temperature is maintained at ~50 °C, while the helium carrier gas pressure and opening time of the valve are optimized to reduce the degree of clustering of the parent ion relative to the parent ion monomer. A typical opening time for the valve is ~13 μs. The molecular beam machine consists of differentially pumped source and interaction chambers, partitioned by a skimmer with a 2 mm aperture. The pulsed valve is housed within the source chamber, whilst the interaction chamber contains VMI optics, replicating the arrangement

described by Eppink and Parker.[43] Generated cations are then accelerated towards a position sensitive detector (under VMI focusing conditions) which consists of a pair of 40 mm diameter chevron microchannel plates (MCPs) coupled to a P-43 phosphor screen (Photek, VID-240). A timed voltage pulse is applied to the rear MCP to gate the detector for measuring only the H^+ or D^+ signal. A 2-D projection of the 3-D ion distribution is subsequently obtained by capturing the light emitted from the phosphor screen using a charge-coupled device (Basler, A-312f). 1-D radial/velocity spectra of the REMPI probed H or D atoms (H^+ or D^+) are obtained through deconvolution of the recorded H^+ or D^+ images by incorporating a polar onion-peeling method[45] into our data acquisition program coded in LabVIEW. Finally, total kinetic energy release (TKER) spectra are obtained from the derived 1-D radial (r) spectra by using an appropriate Jacobian ($r^2 \propto$ KE), assuming the mass of the radical co-fragment is C_4H_4N (66 amu), and a KE calibration factor (obtained by photolysis of HBr at 200 nm[46]).

Alternatively, TR-IY measurements of the total H^+ or D^+ signal, as a function of Δt, can be recorded by monitoring the current output directly from the phosphor screen using an oscilloscope,[47] which is interfaced to our data acquisition program with a general purpose interface bus. This enables a time-of-flight mass spectrum to be recorded at each Δt. Individual mass spectra at each Δt are acquired over ~1250 laser shots, and the measured total H^+ or D^+ signal is then integrated. Resultant TR-IY transients are the average of 20 individual time-resolved scans.

Pyrrole-d_1 was synthesised using a method similar to that described in ref. 26, by repeated stirring of undeuterated pyrrole in excess D_2O in a light sealed vessel for ~48 h. The pyrrole-d_1 product was then separated from the D_2O, and dried over Na_2CO_3. ^{1}H-NMR spectroscopy was used to check for deuteration (>95%).

In addition to the TR-IY and TR-VMI experiments, a vapour phase UV absorption spectrum was recorded with a commercial UV-Visible absorption spectrometer (Perkin Elmer, Lambda 25, 1 nm resolution) by bubbling helium through a sample of pyrrole and collecting the gas in a fused silica sample cell.

3 Results and discussion

3.1 Excited state dynamics following direct excitation to $1^1\pi\sigma^*$ ($^1A_2$)

a H^+ velocity map image, total kinetic energy release spectrum and recoil anisotropy parameters at 250 nm. The inset in Fig. 2(a) depicts a velocity map image of the H-atoms generated following direct excitation to the $1^1\pi\sigma^*$ ($^1A_2$) state of pyrrole at 250 nm, which are subsequently ionised through 2 + 1 REMPI at 243.1 nm with a time-delayed probe pulse set at $\Delta t = 1.2$ ns. The left half displays the recorded image while the right half corresponds to a reconstructed slice through the centre of the original 3-D velocity distribution, extracted using the polar onion-peeling method.[45] A one-colour (243.1 nm probe only) background image has been subtracted from the presented image, such that the signal corresponds exclusively to H-atoms formed and probed after photolysis at 250 nm. The image contains information about both speed and angular recoil distributions of the photodissociated H-atoms. The radial distance of signal from the centre of the image is proportional to the velocity of the H-atoms, with a clear anisotropic ring appearing at large radius, associated with H-atoms carrying large amounts of KE following photodissociation. The enhanced signal intensity

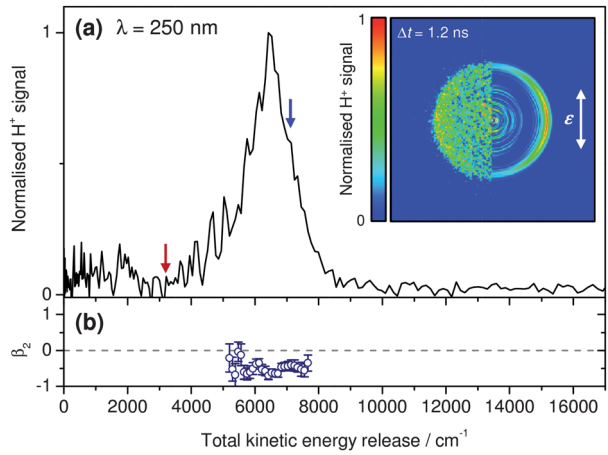

Fig. 2 (a) TKER spectrum and corresponding H^+ velocity map image (inset), obtained following photoexcitation of pyrrole at 250 nm and at a pump–probe delay of $\Delta t = 1.2$ ns. The left half presents the recorded image, while the right half presents a reconstructed slice through the centre of the original 3-D ion distribution (the vertical white arrow indicates the electric field polarisation, $\boldsymbol{\varepsilon}$, of the pump pulse, $h\nu_{pu}$). Vertical blue and red arrows indicate the predicted $TKER_{max}$ values for photodissociation into the $C_4H_4N(\tilde{X})$ + H and $C_4H_4N(\tilde{A})$ + H photoproducts channels, respectively (see Fig. 1(a) and eqn (1)). (b) β_2 recoil anisotropy parameters as a function of TKER between ~5000–8000 cm^{-1} at $\Delta t = 1.2$ ns.

perpendicular to the electric field vector of $h\nu_{pu}$, $\boldsymbol{\varepsilon}$, exhibited by this feature is worthy of note, and indicates that these H-atoms are eliminated on a timescale faster than the rotational timescale of the parent pyrrole molecules; this recoil anisotropy will be discussed further in the ensuing paragraphs.

The TKER spectrum derived from the image is also shown in Fig. 2(a) by the solid black line. This spectrum is dominated by a broad peak centred at ~6500 cm^{-1}, the location of which is in reasonable accord with previous HRA-PTS data by Cronin *et al.*,[27] as well as slice-imaging measurements by Rubio-Lago *et al.*[28] at the same wavelength. However, we concede that the inherently poorer resolution of our ultrafast TR-VMI setup does not allow us to resolve any vibrational mode structure in the TKER distribution. Despite this, we can determine the maximum TKER for dissociation into $C_4H_4N(\tilde{X})$ + H photofragments, $TKER_{max}$, according to the general relationship:

$$TKER_{max} = h\nu_{pu} - D_0(N\text{–}H) - E_{int} \quad (1)$$

In eqn (1) $h\nu_{pu}$ corresponds to the pump photon energy (40000 cm^{-1}), D_0(N–H) is the adiabatic N–H dissociation energy (32850 cm^{-1}),[27] and E_{int} is the total internal (electronic and vibrational) energy of the radical co-fragments. In the case of $C_4H_4N(\tilde{X})$ + H photoproducts with $E_{int} = 0$ cm^{-1}, this returns a value for $TKER_{max}$ of ~7150 cm^{-1}, correlated to a scenario where the $C_4H_4N(\tilde{X})$ co-fragments are formed in their respective zero point vibrational energy level ($v = 0$). This $TKER_{max}$ value is represented by the vertical blue arrow in Fig. 2(a). Within the resolution of our VMI spectrometer,[48] this is in reasonable agreement with the high energy 'tail' of the observed peak centred at ~6500 cm^{-1}, and as such we assign this feature to the formation of $C_4H_4N(\tilde{X})$ + H *via* direct dissociation along $1^1\pi\sigma^*$ ($^1A_2$). In principle, dissociation into C_4H_4N radicals in their first electronic

excited state, $C_4H_4N(\tilde{A})$, together with H, is an energetically open channel at 250 nm. The predicted $TKER_{max}$ for such a channel, using eqn (1) and a calculated $\tilde{A} \leftarrow \tilde{X}$ energy separation of $\sim$3950 cm^{-1},[49] is represented by the vertical red arrow in Fig. 2(a). Based on the very low signal levels observed around 3200 cm^{-1}, we conclude it is unlikely that the $C_4H_4N(\tilde{A})$ + H dissociation channel is accessed at 250 nm, in line with previous observations at the same excitation wavelength.[27,28]

To obtain insight into which modes are promoting the optically forbidden $1^1\pi\sigma^*$ ($^1A_2$) $\leftarrow$ S_0 ($^1A_1$) transition, one can turn to the measured anisotropy parameters, β_2, shown in Fig. 2(b) between $\sim$5000–8000 cm^{-1}. An electronic transition will have greatest intensity when its transition dipole moment ($\boldsymbol{\mu}$) is aligned parallel to $\boldsymbol{\varepsilon}$ (in accordance with a $\cos^2\theta$ distribution, where θ is the angle between $\boldsymbol{\mu}$ and $\boldsymbol{\varepsilon}$[50]). Within the limit of axial recoil and assuming dissociation occurs on a timeframe much faster than molecular rotation (as one anticipates here, given that dissociation is fast following excitation to a dissociative state such as $1^1\pi\sigma^*$ ($^1A_2$)), the distribution in the H-atom photoproducts allows us to ascertain the alignment of the dissociating N–H bond relative to $\boldsymbol{\mu}$. Formally, β_2 can take values between $-1 \leq \beta_2 \leq 2$, where these limiting values of -1 and 2 correspond to scenarios in which the dissociating bond is aligned perpendicular or parallel to $\boldsymbol{\mu}$, respectively. The measured non-limiting (average) value of $\beta_2 \approx -0.5$ in Fig. 2(b) is in good agreement with previous observations,[27,28] which largely report β_2 values of < 0. This suggests that the dominant modes responsible for promoting the transition possess either b_2 or b_1 symmetry, Γ_v, inducing vibronic transition moments of either b_1 or b_2 symmetry, $\Gamma_{\boldsymbol{\mu}}$, (transforming as x and y, respectively, in C_{2v} symmetry) both of which lie perpendicular to the dissociating N–H bond. Such a conclusion is formed on the basis that $A_1 \otimes \Gamma_v \otimes \Gamma_{\mu} \otimes A_2 \supseteq A_1$. However, we note that modes of a_2 symmetry may also promote the $1^1\pi\sigma^*$ ($^1A_2$) $\leftarrow$ S_0 ($^1A_1$) transition, inducing a vibronic transition moment of a_1 symmetry (parallel to the N–H bond), leading to $\beta_2 > 0$ for peaks associated with a_2 vibrations, as observed in the high-resolution TKER spectra reported by Cronin *et al.*[27] The reduced resolution in our broadband ($\sim$500 cm^{-1}) measurements prohibits a similar observation here, although contributions from a_2 vibrations may account for the non-limiting β_2 value of -0.5.

b H-atom elimination dynamics at 250 nm. A normalised TR-IY transient of the *total* H^+ signal as a function of pump–probe delay, between $\Delta t = -1$ ps and 2.5 ps, following photoexcitation at 250 nm and probing at 243.1 nm is shown in Fig. 3(a) (open circles). A 243.1 nm probe only background signal has been subtracted from the displayed transient, noting that negligible 250 nm pump-only signal was observed, in line with 250 nm being non-resonant with the 2s $\leftarrow$ 1s transition in H. At negative pump–probe delays ($\Delta t < 0$), an appreciable 'probe-pump' H^+ signal is observed. This concurs with observations in earlier TR-IY measurements conducted at 250 nm by Lippert *et al.*,[22] and we discuss the origins of this signal in greater detail below. Around $\Delta t = 0$, a sharp rise in signal is observed, which then decays within our IRF (<120 fs). Upon increasing the time delay to positive pump–probe delays ($\Delta t > 0$), the signal then steadily rises before plateauing around $\sim$500 fs.

Unlike previous studies by Lippert *et al.*[22] however, we have additionally performed TR-VMI measurements to generate a series of complementary time-resolved TKER spectra at a series of Δt between -1 ps and 1.2 ns, presented in Fig. 3(b). At $\Delta t = -1$ ps a small feature centred at $\sim$7000 cm^{-1} is observed, which

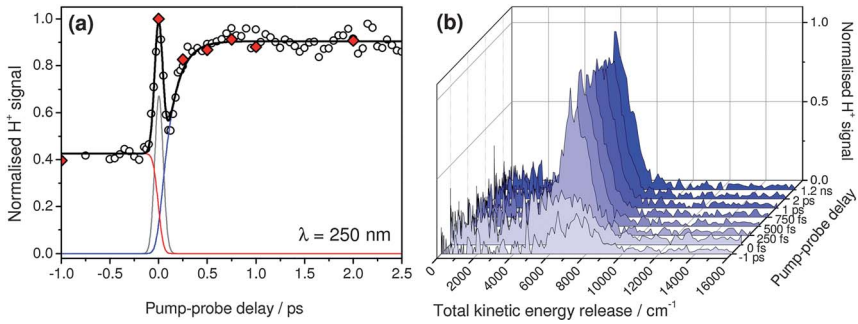

Fig. 3 (a) Normalised H^+ signal transient obtained using TR-IY (open circles), with a 250 nm pump and 243.1 nm probe combination, together with the resultant kinetic fit (black line). A one-colour 243.1 nm background signal has been subtracted from the displayed transient. Individual fit components associated with $\tau_f = 126$ fs (blue), $\tau_r < 30$ fs (red) and $\tau_d < 30$ fs (grey) are also shown (see main text for details). (b) Background (243.1 nm probe only) subtracted time-resolved TKER spectra, at a series Δt, following excitation at 250 nm. The total integrated H^+ signal in each time-resolved TKER spectrum is shown superimposed on (a) as red diamonds.

then moves towards lower TKER ($\sim$6500 cm^{-1}) and significantly broadens in width at $\Delta t = 0$. In addition, there is also a notable increase in signal at low TKER (<4000 cm^{-1}) at this pump–probe delay, which exhibits a broad profile. By $\Delta t =$ 500 fs, a new narrower feature centred at $\sim$6500 cm^{-1} has appeared, correlated to probed H-atoms formed following N–H dissociation along the $1^1\pi\sigma^*$ ($^1A_2$) surface at 250 nm, as discussed above (*cf.* Fig. 2(a)). This feature exhibits a constant intensity out to $\Delta t = 1.2$ ns, with no significant signal at low TKER (<4000 cm^{-1}) in any spectra recorded at $\Delta t \geq 250$ fs. This latter observation instils confidence that the rapid (sub-500 fs) rise in signal observed at positive pump–probe delays in Fig. 3(a), correlates (almost) exclusively to direct $1^1\pi\sigma^*$ ($^1A_2$) mediated N–H bond scission, with negligible contributions from slower statistical H-atom elimination from hot S_0 species (by 1.2 ns), following IC back to S_0 at the $1^1\pi\sigma^*/S_0$ CI (*vide infra*). Agreement between the TR-VMI and TR-IY measurements is confirmed by overlaying the normalised total integrated H^+ signal in each of the time-resolved TKER spectra on top of the normalised TR-IY trace (red diamonds, Fig. 3(a)), showing excellent agreement with each other.

In order to extract a time-constant for the appearance of H-atoms eliminated along the $1^1\pi\sigma^*$ ($^1A_2$) at 250 nm, the H^+ signal transient in Fig. 3(a) is fitted to the sum of an exponential rise (τ_f) and decay (τ_d) function at positive Δt, and a single exponential rise function (τ_r) at negative Δt. All three functions are convolved with our Gaussian IRF of 120 fs. The reader is referred to the electronic supplementary information (ESI†) online for further details of the kinetic fitting procedure. The result of this fit is shown as the solid black line through the experimental data points in Fig. 3(a). The time-constants returned from the kinetic fit have values of $\tau_f = 126 \pm 28$ fs, $\tau_d < 30$ fs and $\tau_r < 30$ fs; these individual fit components are indicated by the blue, grey and red lines in Fig. 3(a), respectively. The minimum temporal resolution of our measurements is $\sim$30 fs ($\sim$25% of our 120 fs Gaussian IRF)[7] and as a result we quote values for both τ_d and τ_r as <30 fs. τ_r is attributed to 'reverse dynamics', discussed further below. τ_d corresponds to the decay of the peak present in the H^+ transient around $\Delta t = 0$, and arises due to multiphoton

processes mediated by the increased photon flux when the pump and probe pulses are temporally overlapped, which may yield H^+ directly (*e.g.* dissociative ionisation), as seen in our previous studies on other aromatic heterocycles.[6,10,51,52] The rapid decay of this signal after $\Delta t = 0$ is merely a reflection of the extremely short lived nature of the resonant intermediate state that promotes this multi-photon process. Finally, the remaining component of the fit, $\tau_f = 126 \pm 28$ fs, is attributed to the appearance timescale of (REMPI probed) H-atoms formed through photoexcitation to and N–H dissociation along the $1^1\pi\sigma^*$ ($^1A_2$) surface at 250 nm.

It is worth noting the disparity in the time-constants for the forward ($\tau_f = 126 \pm 28$ fs) and reverse ($\tau_r < 30$ fs) dynamics. The forward dynamics result from single photon excitation with 250 nm to the $1^1\pi\sigma^*$ ($^1A_2$) state which subsequently dissociates to yield H-atoms probed through 2+1 REMPI with 243.1 nm. In contrast, the reverse dynamics correspond to single photon excitation with 243.1 nm to the $1^1\pi\sigma^*$ ($^1A_2$) state, forming H-atoms which are then two-photon excited with 243.1 nm to the 2s level. These excited H(2s)-atoms are then ionised with a single photon of 250 nm to yield H^+. Such an interpretation of these reverse dynamics has also previously been put forward by Lippert *et al.*[22] The disparity between the values of τ_f and τ_r therefore most likely reflects the different mechanisms *via* which H^+ is generated at $\Delta t < 0$ and $\Delta t > 0$: for the reverse dynamics, photodissociation of the N–H bond *and* two-photon excitation of the 2s $\leftarrow$ 1s transition all needs to occur within the temporal width of the 243.1 nm pulse ($\sim$80 fs), hence giving rise to the very fast time-constant of $\tau_r < 30$ fs – this is not the case for the forward dynamics. In further support of the 'probe-pump' mechanism proposed for forming H^+ at $\Delta t < 0$, we recall the fact that the feature observed in the TKER spectrum at $\Delta t = -1$ ps is centred at $\sim$7000 cm^{-1}, whereas the pronounced peak in the spectra recorded at $\Delta t \geq 250$ fs is centred at $\sim$6500 cm^{-1}. The blue-shift in central TKER of the feature observed at $\Delta t = -1$ ps, relative to the spectra at $\Delta t \geq 250$ fs in Fig. 3(b), is a direct reflection of the increased photon energy imparted to the $1^1\pi\sigma^*$ ($^1A_2$) state at 243.1 nm (compared to 250 nm), enabling more of the available energy to be partitioned into TKER during the N–H fission process.

As this stage, we highlight one key difference between the H^+ transient presented here and those reported earlier by Lippert *et al.*[22] Unlike the results presented in Fig. 3(a), these authors measured a H^+ signal transient which exhibited a bi-exponential rise profile with two time-constants, τ_1 and τ_2, with values of 110 ± 80 fs and 1.1 ± 0.5 ps, respectively.[22] Although τ_1 compares very favourably with our measured value of $\tau_f = 126 \pm 28$ fs, we do not observe any evidence of a second slower rise in our H^+ signal correlating to τ_2 ($\sim$1.1 ps). Lippert *et al.* speculated that the latter time-constant of 1.1 ps, arose through some fraction of the dissociating wavepacket non-adiabatically coupling back into a vibrationally hot S_0 state, which may then undergo N–H dissociation to yield a 'statistical' distribution of slower H-atoms. We observe negligible H-atoms with a statistical distribution in our time-resolved TKER spectra out to $\Delta t = 1.2$ ns (Fig. 3(b)). This also accords with the high-resolution TKER spectrum measured by Cronin *et al.* at 250 nm ($\Delta t \sim 5$ ns),[27] although we acknowledge that Rubio-Lago *et al.* do observe a reasonable fraction of H-atoms with a statistical profile at the same wavelength.[28] Such a distribution can, however, arise from undesired multiphoton dissociative ionisation events, which may appear on an ultrafast (<200 fs) timeframe.[14,51,53,54]

Additionally, in previous TR-VMI studies on related aromatic heterocycles (imidazole and pyrazole) at 200 nm,[11] as well as in the present work on pyrrole (see section 3.2), we have indeed observed evidence for the onset of statistical H-atom elimination from hot S_0 species, but taking place on a much longer timeframe of hundreds of picoseconds to nanoseconds. Ultimately, the preceding arguments and our present findings open a debate as to what role, if any, does a statistical H-atom elimination pathway play in the photophysics of pyrrole at 250 nm within ~1 ns? – at present this remains somewhat unclear based on the conflicting experimental data.

c The role of tunnelling on the $1^1\pi\sigma^*$ ($^1A_2$) surface at 250 nm. The value of $\tau_f = 126 \pm 28$ fs, while still ultrafast, is perhaps longer than one might anticipate for the appearance of H-atoms, following direct excitation to a state such as $1^1\pi\sigma^*$ ($^1A_2$) in pyrrole, given its repulsive profile with respect to R_{N-H}. Lippert *et al.*[22] also briefly acknowledged this fact at 250 nm, and suggested that this may be due to the dissociating wavepacket being impeded by a small exit barrier to N–H fission, which lies close to the vertical Franck–Condon region in $1^1\pi\sigma^*$ ($^1A_2$) state. With reference to Fig. 4(a), this exit barrier arises from the fact that the effective 'adiabatic' $1^1\pi\sigma^*$ ($^1A_2$) surface, shown by the solid black line, corresponds to the lower adiabat formed through an avoided-crossing between the diabatic $^1\pi$3s Rydberg and $^1\pi\sigma^*$ valence states (dotted grey lines).[55,56] Previous theoretical calculations predict the energy (height) of the exit barrier to be between ~240–3200 cm^{-1},[29,33] although to date, no direct experimental evidence for this exit barrier has been reported. Nonetheless, by analogy with σ* mediated N–H bond fission dynamics observed in related systems, such as ammonia[57] and aniline (aminobenzene),[56] following excitation into the quasi-bound 3s Rydberg well of the $1^1\pi\sigma^*$ ($^1A_2$) state, it could be possible for population to escape *via* tunnelling through this exit barrier and evolve towards N–H dissociation. Fig. 4(a) shows a reduced 1-D picture for this tunnelling mechanism at 250 nm along R_{N-H}, originating from the zero-point of the N–H stretch ($v_{NH} = 0$) in a (vibrationally excited)

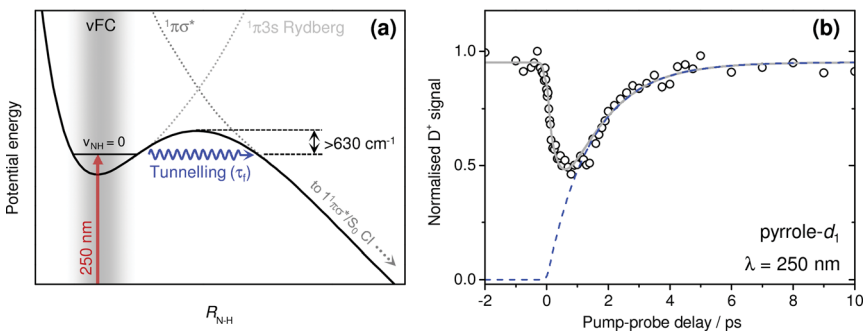

Fig. 4 (a) Enlarged schematic of the 'adiabatic' $1^1\pi\sigma^*$ ($^1A_2$) surface (solid black line) in pyrrole as a function of R_{N-H}. The diabatic $^1\pi$3s Rydberg and $^1\pi\sigma^*$ valence surfaces are also shown by the dotted grey lines. Excitation into the quasi-bound 3s Rydberg well (in the vertical Franck–Condon (vFC) region; grey shading) of a (vibrationally excited) adiabatic $1^1\pi\sigma^*$ ($^1A_2$) surface at 250 nm is shown by the red arrow. Tunnelling through the exit barrier onto the dissociative region of this potential is shown by the blue arrow. (b) Normalised D^+ signal transient obtained using TR-IY (open circles), following photolysis of pyrrole-d_1 with a 250 nm pump and 243.1 nm probe combination. The $\tau_f = 1.4$ ps fit (dashed blue line) is also shown (see ESI† for details). The grey line is provided as a visual guide.

adiabatic $1^1\pi\sigma^*$ ($^1A_2$) potential. Such a tunnelling mechanism would most likely impede N–H fission dynamics, and account for the slightly longer value of $\tau_f = 126 \pm 28$ fs we measure here at 250 nm.

To investigate whether such a tunnelling mechanism is active following excitation to the $1^1\pi\sigma^*$ ($^1A_2$) surface at 250 nm, we have also performed TR-IY measurements on the *total* D^+ signal as a function of Δt, after photolysis of pyrrole-d_1 at the same wavelength. The results of these measurements are presented in Fig. 4(b) (open circles). The D^+ signal transient bears some similarities to the H^+ transient in Fig. 3(a), although there is no obvious sharp 'spike' in D^+ signal around $\Delta t = 0$, suggesting that the spike observed at $\Delta t = 0$ in Fig. 3(a) has significant contributions from multiphoton-driven C–H fission. However, perhaps the most striking difference is the significantly slower rise in the D^+ signal at $\Delta t > 0$, which does not plateau until ~6 ps. A kinetic fit, obtained by fitting to the *rising* D^+ signal at $\Delta t \geq 1$ ps only (see ESI† for details), is shown by the dashed blue line in Fig. 4(b). This fit returns a value of $\tau_f = 1.4 \pm 0.3$ ps, and in turn yields a kinetic isotope effect (k_H/k_D) of ~11. Such a large kinetic isotope effect strongly supports the idea that following excitation at 250 nm, N–H bond fission proceeds *via* tunnelling through a small exit barrier in the $1^1\pi\sigma^*$ ($^1A_2$) surface. This is, to the best of our knowledge, the first experimental evidence that the $1^1\pi\sigma^*$ ($^1A_2$) surface in pyrrole does indeed possess a quasi-bound well in the vertical Franck–Condon region, and that population can evolve out of it *via* tunnelling. Based on previous HRA-PTS measurements by Cronin *et al.*,[27] who report that the origin band of the $1^1\pi\sigma^*$ ($^1A_2$) state must lie at >254 nm, and our measurements here at 250 nm, we conclude that the exit barrier to N–H dissociation in this state must be >630 cm^{-1}.

d H-atom elimination dynamics at 238 nm: effects of excess internal energy. We now consider the effect of increasing excitation energy on the observed dynamics, after direct excitation to $1^1\pi\sigma^*$ ($^1A_2$). The inset in Fig. 5(a) contains a velocity map image of H-atoms generated following excitation at 238 nm to the $1^1\pi\sigma^*$ ($^1A_2$) state, which is probed with a time-delayed 243.1 nm probe ($\Delta t = 1.2$ ns). The left half of the image once again displays the collected image (after one-colour 243.1 nm background subtraction) while the right half presents a reconstructed slice through the centre of the original 3-D H^+ distribution. As with photoexcitation at 250 nm, there is a clear anisotropic feature ($\beta_2 \approx -0.4$, see Fig. S1 of the ESI†) at large radius, corresponding to photodissociated H-atoms born with large amounts of KE. The similarities between both images in Fig. 3(a) and 5(a) indicate that these H-atoms are indeed formed *via* similar mechanisms – *i.e.* $1^1\pi\sigma^*$ ($^1A_2$) mediated N–H bond fission.

Further similarities/differences between excitation at 250 and 238 nm can be gleaned through the corresponding time-resolved TKER spectra and H^+ signal transient, which are shown in Fig. 5(a) and 5(b), respectively. As with the measurements at 250 nm, the TKER spectrum at $\Delta t = -5$ ps displays a small amount of signal peaked at ~7000 cm^{-1}, and can analogously be assigned to N–H bond cleavage along $1^1\pi\sigma^*$ ($^1A_2$) at 243.1 nm, where the time-delayed 238 nm photons are involved in the H-atom ionisation step. Cursory inspection of the TKER spectrum in Fig. 2(a) and those at $\Delta t = 1$ ps and 1.2 ns in Fig. 5(a), clearly reveals a difference in the peak position of the feature at high TKER when excited at 250 and 238 nm, respectively. For excitation at 250 nm the feature appears centred at ~6500 cm^{-1}, whereas at 238 nm it appears at ~7200 cm^{-1} due to the

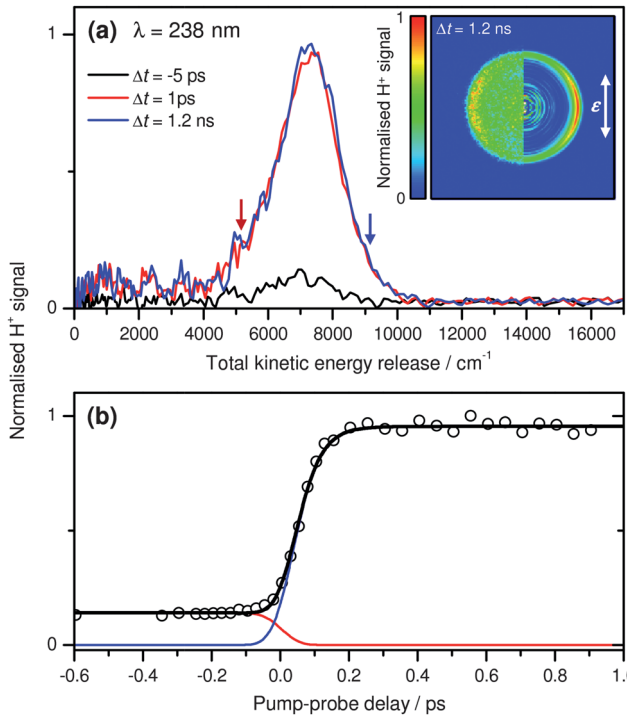

Fig. 5 (a) Time-resolved TKER spectra recorded following photoexcitation of pyrrole at 238 nm, and probing H-atoms with a time-delayed 243.1 nm pulse. Vertical arrows indicate the predicted $TKER_{max}$ values for N–H dissociation into the $C_4H_4N(\tilde{X})$ + H (blue) and $C_4H_4N(\tilde{A})$ + H (red) photoproduct channels (see Fig. 1(a) and eqn (1)). Inset: H^+ velocity map image (left) and reconstructed slice through the centre of the original 3-D ion distribution (right), recorded at $\Delta t = 1.2$ ns (white arrow indicates the polarisation of $h\nu_{pu}$). (b) Integrated H^+signal transient (6000–8500 cm^{-1}), following excitation at 238 nm (open circles), together with an associated kinetic fit (black line). Individual fit components associated with $\tau_f =$ 46 fs (blue) and $\tau_r < 30$ fs (red) are also shown (see main text for details).

increased photon energy. Similarly, the feature at ~7200 cm^{-1} is assigned to dissociation into $C_4H_4N(\tilde{X})$ + H photoproducts *via* the $1^1\pi\sigma^*$ ($^1A_2$) surface at 238 nm, confirmed through agreement between the predicted $TKER_{max}$ for this channel (~9170 cm^{-1} at 238 nm) and the location of the high energy tail of this feature (vertical blue arrow, Fig. 5(a)). No significant signal associated with the higher energy $C_4H_4N(\tilde{A})$ + H photoproduct channel is observed in Fig. 5(a). We also note that N–H dissociation dynamics along the $1^1\pi\sigma^*$ ($^1A_2$) surface appear complete by $\Delta t = 1$ ps, as there is no further evolution of the amplitude of the high TKER feature between 1 ps and 1.2 ns, in line with direct excitation to a dissociative state.

The H^+ signal transient in Fig. 5(b) (open circles) is obtained by integrating the high TKER feature (6000–8500 cm^{-1}) in TKER spectra recorded at many Δt values between −0.6 to 1 ps, and enables a more quantitative analysis of the timescale for H-atom elimination along $1^1\pi\sigma^*$ ($^1A_2$) at 238 nm. Using a similar approach to that described in section 3.1b, time-constants of $\tau_f = 46 \pm 22$ fs and $\tau_r < 30$ fs, are extracted *via* a kinetic fit (black line); the τ_f and τ_r components of the fit are shown by the blue and red lines in Fig. 5(b), respectively. Unlike the data at 250 nm

(Fig. 3(a)), there is no noticeable 'spike' in the measured H^+ signal around $\Delta t = 0$. This may suggest that an appropriate intermediate state, which can undergo dissociative ionisation to yield H^+, is not accessible *via* multiphoton excitation at this combination of pump and probe wavelengths, although unlike TR-IY measurements at 250 nm (Fig. 3(a)), the transient in Fig. 5(b) is obtained by integrating *only* signal associated with $1^1\pi\sigma^*$ ($^1A_2$) driven N–H fission. Reassuringly, τ_r once again yields a time-constant that is faster than our IRF (<30 fs), and can be reconciled with the mechanism outlined above (see section 3.1b).

We draw this section to a close by pointing the reader's attention to the notable difference in the τ_f values extracted following excitation at 250 and 238 nm; $\tau_f = 126 \pm 28$ fs and 46 ± 22 fs, respectively. At 250 nm we concluded that N–H bond fission proceeds by population tunnelling out of the small quasi-bound 3s Rydberg well in the vertical Franck–Condon region of the $1^1\pi\sigma^*$ ($^1A_2$) surface, giving rise to a H-atom appearance time-constant which is slower than one might traditionally anticipate if N–H fission occurred in a purely 'ballistic' fashion along a highly repulsive surface. At 238 nm, the time-constant of $\tau_f = 46 \pm 22$ fs is ~3 times faster than at 250 nm, suggesting that direct excitation to $1^1\pi\sigma^*$ ($^1A_2$) at this wavelength is above the exit barrier and N–H fission occurs directly, rather than *via* tunnelling. Indeed, TR-IY measurements on pyrrole-d_1, which monitor the *total* D^+ signal as a function of Δt at 238 nm, return a time-constant of $\tau_f = 136 \pm 38$ fs for the appearance of D-atoms formed *via* N–D fission along $1^1\pi\sigma^*$ ($^1A_2$) (see Fig. S2 of the ESI†). This returns a much smaller kinetic isotope effect of ~2.9, which indicates that tunnelling plays a negligible role in the H-atom elimination dynamics at 238 nm in pyrrole, resulting in very rapid N–H bond fission within 46 ± 22 fs.

3.2 Excited state dynamics following excitation to $^1\pi\pi^*$ ($^1B_2$) at 200 nm

a Time-resolved total kinetic energy release spectra. We now turn our attention to dynamics occurring following photoexcitation of the $^1\pi\pi^*$ ($^1B_2$) state at 200 nm. Time-resolved TKER spectra recorded following H-atom elimination from pyrrole at 200 nm are shown in Fig. 6(a) at $\Delta t = -5$ ps (black), 1 ps (blue) and 1.2 ns (red). Reconstructed slices through the centre of the original 3-D H^+ distributions at $\Delta t = 1$ ps (left) and 1.2 ns (right) are also shown in inset. At 200 nm, no 'probe-pump' signal is observed at $\Delta t = -5$ ps, indicating an absence of reverse dynamics. As with measurements at 250 and 238 nm, both TKER spectra at $\Delta t > 0$ once again clearly display an intense feature at high TKER, peaked around ~7200 cm^{-1}, correlated with the anisotropic signal ($\beta_2 \approx -0.5$, see Fig. S3 of the ESI†) at large radii in the inset velocity map images. Unlike measurements at longer wavelengths however (section 3.1), this feature at 200 nm exhibits a pronounced tail which decays in intensity towards higher TKER, returning to the baseline signal level between ~16000–17000 cm^{-1}. The predicted $TKER_{max}$ values for dissociation into the three possible photoproduct channels (see Fig. 1(a)) after N–H bond scission at 200 nm are shown by the blue, red and light brown arrows, respectively, in Fig. 6(a); $TKER_{max}$ for the higher energy $C_4H_4N(\tilde{B})$ + H photoproduct channel (light brown arrow) is determined using eqn (1) and a calculated $\tilde{B} \leftarrow \tilde{X}$ energy separation of ~10400 cm^{-1}.[58] Unfortunately, given the spectral bandwidth of the fs pump pulse (~500 cm^{-1}) and the restricted resolution of our VMI spectrometer,[48] it is challenging to identify which electronic

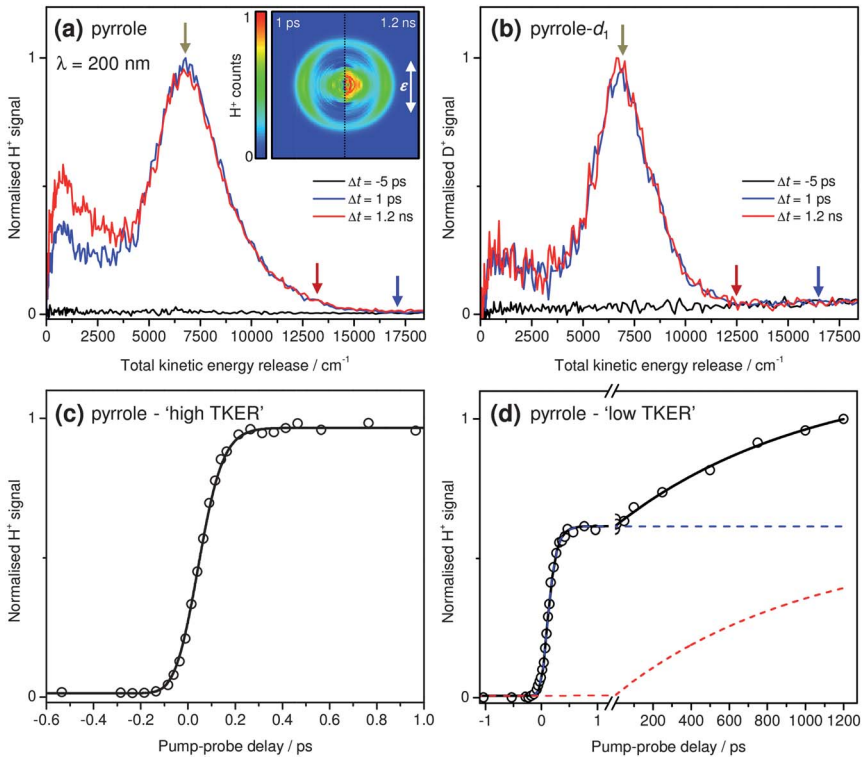

Fig. 6 (a), (b) Time-resolved TKER spectra recorded following photoexcitation of pyrrole and pyrrole-d_1 at 200 nm, and probing H/D-atoms with a time-delayed 243.1 nm pulse, respectively. Vertical arrows indicate the predicted $TKER_{max}$ values for N–H dissociation into the $C_4H_4N(\tilde{X})$ + H (blue), $C_4H_4N(\tilde{A})$ + H (red) and $C_4H_4N(\tilde{B})$ + H (light brown) photoproduct channels (see Fig. 1(a) and eqn (1)). Inset in (a): Reconstructed slices through the centre of the original 3-D H^+ distribution at $\Delta t = 1$ ps (left) and 1.2 ns (right). The white arrow indicates the polarisation of $h\nu_{pu}$. (c) Integrated 'high TKER' H^+ signal transient (5000–10000 cm^{-1}), following excitation of pyrrole at 200 nm (open circles), together with an associated kinetic fit with a single component of $\tau_f = 52$ fs (black line). (d) Integrated 'low TKER' H^+ signal transient (200–3000 cm^{-1}), following excitation of pyrrole at 200 nm (open circles), together with an associated kinetic fit (black line). Individual fit components associated with $\tau_L = 108$ fs (dashed blue line) and $\tau_{stat} = 1.0$ ns (dashed red line) are also shown (see main text for details).

state the pyrrolyl co-fragments are formed in. Previous high-resolution HRA-PTS measurements at 193.3 nm by Cronin *et al.*[27] do, however, allow an excellent comparative insight into the branching between the three possible photoproduct channels at 200 nm, and strongly suggests that only the $C_4H_4N(\tilde{X})$ + H channel is populated. With reference to Fig. 1(a), this implies that flux does not couple directly from the $^1\pi\pi^*$ ($^1B_2$) state onto the higher lying $2^1\pi\sigma^*$ ($^1B_1$) state (*via* a $^1\pi\pi^*/2^1\pi\sigma^*$ CI), the diabatic asymptote of which is correlated with the $C_4H_4N(\tilde{A})$ + H channel, even though such a pathway is proposed to be energetically open by 200 nm.[58] We therefore propose that the high TKER feature *predominantly* arises through flux coupling onto the $1^1\pi\sigma^*$ ($^1A_2$) state from the initially populated $^1\pi\pi^*$ ($^1B_2$) state, *via* an appropriate $^1\pi\pi^*/1^1\pi\sigma^*$ CI (located along a 'ring-distortion' coordinate orthogonal to R_{N-H}),[30–33] followed by subsequent N–H bond cleavage to yield $C_4H_4N(\tilde{X})$ + H photoproducts. We acknowledge however, that it is not

possible to definitively rule out initial population of other electronic excited states at 200 nm, particularly the $^1\pi\pi^*$ ($^1A_1$) state, which is thought to contribute ~15% of the total observed absorbance in pyrrole's first strong absorption band (see Fig. 1(b)).[26,39] The non-limiting β_2 value of −0.5 associated with the high TKER feature in Fig. 6(a), provides some evidence that this may indeed be the case: for the stronger $^1\pi\pi^*$ ($^1B_2$) ← S_0 ($^1A_1$) transition, $\boldsymbol{\mu}_y$ (b_2 symmetry) is aligned perpendicular to the N–H bond, while for $^1\pi\pi^*$ ($^1A_1$) ← S_0 ($^1A_1$) excitation $\boldsymbol{\mu}_z$ (a_1 symmetry) is aligned parallel to the N–H bond, a superposition of which may yield a non-limiting negative β_2 value of −0.5.[59]

In contrast to the TKER spectra recorded after direct excitation to $1^1\pi\sigma^*$ ($^1A_2$), the spectra at $\Delta t > 0$ in Fig. 6(a) contain a significant fraction of signal at <4000 cm^{-1}, with a 'Boltzmann-like' profile peaked at ~1000 cm^{-1}. At 250 and 238 nm such signal contributions are minimal (Fig. 2(a) and 5(a)). Furthermore, what is perhaps most striking is the clear time dependence of the intensity of this 'low TKER' feature, as evidenced by the change in signal level below ~4000 cm^{-1} between $\Delta t = 1$ ps (blue) and 1.2 ns (red), which is clearly absent in the high TKER feature. This is also clearly seen in the associated time-resolved velocity map images (Fig. 6(a), inset) as an enhanced number of H^+ counts near to the centre of the image. In order to ascertain the origins to this slower rise in signal at low TKER, we have performed comparative studies on pyrrole-d_1. These measurements enable a clear determination of whether these H-atoms at low TKER are born through either N–H or C–H bond fission, or both. Time-resolved TKER spectra recorded at $\Delta t = -5$ ps (black), 1 ps (blue) and 1.2 ns (red) after 200 nm excitation of pyrrole-d_1 are shown in Fig. 6(b). These spectra were obtained by imaging D^+, rather than H^+, following 2+1 REMPI of any eliminated D-atoms at 243.1 nm. The feature at high TKER is peaked at slightly lower energy (~7000 cm^{-1}), in line with the stronger N–D bond strength (D_0(N–D) ~33600 cm^{-1}).[60,61] Additionally, the high energy tail of this feature only extends to ~12500 cm^{-1} some ~3500–4500 cm^{-1} less than that observed in undeuterated pyrrole (Fig. 6(a)). This indicates that, on average, the $C_4H_4N(\tilde{X})$ co-fragments retain more of the available excess energy as internal (vibrational) energy following N–D bond fission, relative to N–H bond fission in undeuterated pyrrole. However, what is most revealing is the apparent invariance in the amplitude of the low TKER component as a function of Δt, compared to measurements on the undeuterated counterpart. Unlike the spectra presented in Fig. 6(a), which may, in principle, possess signal components from both N–H *and* C–H bond dissociation, the signal in Fig. 6(b) can only arise from N–D bond scission. Therefore, given that the low TKER component in Fig. 6(b) does not increase between $\Delta t = 1$ ps and 1.2 ns we can, with reasonable confidence, exclusively attribute the rise in signal at low TKER when $\Delta t > 1$ ps in Fig. 6(a) to a mechanism involving C–H bond cleavage. We discuss the precise nature of this C–H fission mechanism in greater detail below (section 3.2c).

b H-atom elimination dynamics *via* the $1^1\pi\sigma^*$ ($^1A_2$) surface. Timescales for H-atom elimination dynamics at 200 nm are extracted from normalised integrated H^+ signal transients for both the high TKER (5000–10000 cm^{-1}) and low TKER (200–3000 cm^{-1}) features, presented in Fig. 6(c) and 6(d), respectively (open circles). We initially consider the high TKER H^+ signal transient in Fig. 6(c), presented between $\Delta t = -0.6$ to 1 ps. Beyond $\Delta t = 1$ ps the signal associated with the high TKER component plateaus, as evidenced by the time-resolved TKER

spectra in Fig. 6(a). Unlike the H^+ signal transients obtained at 238 and 250 nm excitation, no reverse dynamics are observed at 200 nm and only a single time-constant of $\tau_f = 52 \pm 12$ fs is required to fit the data (black line), which is assigned as the overall timescale for a $^1\pi\pi^*$ ($^1B_2$) $\rightarrow$ $1^1\pi\sigma^*$ ($^1A_2$) $\rightarrow$ N–H fission mechanism to take place. Such a mechanism is based on/supported by conclusions drawn in previous experimental work.[24,26,27] This value for τ_f is similar to that obtained following 238 nm excitation (46 $\pm$ 22 fs), and the implications of this are discussed below.

From a theoretical perspective, mixed quantum-classical dynamics simulations by Barbatti and co-workers[32,33] predict that $\sim$80% of the initial $^1\pi\pi^*$ ($^1B_2$) state population is deactivated *via* $^1\pi\pi^*$ ($^1B_2$) $\rightarrow$ $1^1\pi\sigma^*$ ($^1A_2$) coupling, and return an *average* timescale of 54 fs for the onset of N–H bond dissociation along $1^1\pi\sigma^*$ ($^1A_2$),[32] in excellent accord with our reported appearance timescale of 52 $\pm$ 12 fs for high TKER H-atoms at 200 nm. Given the measured value for τ_f at 200 nm, we can conclude that population transfer in the initial $^1\pi\pi^*$ ($^1B_2$) $\rightarrow$ $1^1\pi\sigma^*$ ($^1A_2$) IC step must take place within a sub-50 fs timeframe. Once again, theory[32] predicts that coupling through appropriate CIs, located along ring deformation coordinates,[30–33] occurs within $\sim$20 fs. Furthermore, we also draw on recent ultrafast TR-IY studies on the pyrrole cation (pyrrole$^+$) signal by Montero *et al.*,[23] who report a timescale of 19 $\pm$ 3 fs for the initial $^1\pi\pi^*$ ($^1B_2$) $\rightarrow$ $1^1\pi\sigma^*$ ($^1A_2$) IC process, in good agreement with both our current observations and previous dynamics simulations. However, after direct excitation of $1^1\pi\sigma^*$ ($^1A_2$) at 238 nm we measure a value for τ_f of 46 $\pm$ 22 fs, which is very comparable to the value of 52 $\pm$ 12 fs extracted at 200 nm. In principle, one may anticipate that H-atoms born through a $^1\pi\pi^*$ ($^1B_2$) $\rightarrow$ $1^1\pi\sigma^*$ ($^1A_2$) $\rightarrow$ N–H fission pathway at 200 nm will possess a longer appearance timescale than those formed after direct excitation to $1^1\pi\sigma^*$ ($^1A_2$), given the additional time ($\sim$20 fs) required for the initial $^1\pi\pi^*$ ($^1B_2$) $\rightarrow$ $1^1\pi\sigma^*$ ($^1A_2$) step. Such a timescale is within the statistical uncertainty ($\pm$22 fs) of the extracted τ_f value at 238 nm, and we postulate that this, together with the increased kinetic energy of the dissociating wavepacket, is the most likely origin of such a discrepancy.

c Statistical H-atom elimination dynamics. We now return to discuss the low TKER H^+ signal transient depicted in Fig. 6(d). In stark contrast to the high TKER H^+ signal transient, the temporal profile of the H^+ signal at low TKER clearly exhibits a bi-exponential rise, occurring within two very different time-constants. Moreover, the slower rise in signal at low TKER has not plateaued by the maximum temporal delay achievable in our current experiments (Δt = 1.2 ns), suggesting that these dynamics are incomplete by 1.2 ns. This H^+ signal transient can be fitted using two exponential rise functions (black line), which returns time-constants of $\tau_L = 108 \pm 20$ fs (dashed blue line) and $\tau_{stat} = 1.0 \pm 0.4$ ns (dashed red line). Analogous to conclusions drawn in previous work on related aromatic heterocycles,[10,51,53,54] we attribute the τ_L time-constant to the appearance timescale for H-atoms formed *via* undesired multiphoton induced pathways; such a result is not a central discussion point in this paper and the reader is referred to the aforementioned references for further details. We now move on to discuss the origins of the $\tau_{stat} = 1.0 \pm 0.4$ ns time-constant in the ensuing paragraphs.

Theoretical calculations can provide an excellent starting point for discussing the $\tau_{stat} = 1.0 \pm 0.4$ ns time-constant extracted from the low TKER H^+ signal transient in Fig. 6(d). As mentioned above in section 3.2b, $\sim$80% of the initial

population imparted to $^1\pi\pi^*$ ($^1B_2$) is predicted to decay *via* coupling onto the lower lying $1^1\pi\sigma^*$ ($^1A_2$) surface.[32,33] However, the remaining population can directly couple back onto S_0 at appropriate $^1\pi\pi^*/S_0$ CIs,[30–33] or evolve towards alternative photofragmentation pathways (*e.g.* HCN + C_3H_4), the latter of which has been experimentally observed by Blank *et al.* at 193 nm;[24] we focus on the former as a pathway for forming H-atoms at low TKER. It was postulated in these theoretical studies,[32,33] that low TKER H-atoms could be generated through population of vibrationally hot S_0 pyrrole molecules, which subsequently undergo statistical unimolecular dissociation on a timeframe significantly longer than ultrafast N–H bond fission along the $1^1\pi\sigma^*$ ($^1A_2$) surface. IC from $^1\pi\pi^*$ ($^1B_2$) $\rightarrow$ S_0, mediated at an appropriate CI along a ring-distortion coordinate, offers one viable pathway for forming hot S_0 species, which can then eject statistical H-atoms with low TKER. Alternatively, after IC from $^1\pi\pi^*$ ($^1B_2$) $\rightarrow$ $1^1\pi\sigma^*$ ($^1A_2$), population can access the $1^1\pi\sigma^*/S_0$ CI at extended R_{N-H} distances, also providing a route to forming hot S_0 molecules, ultimately yielding low TKER H-atoms (see PECs in Fig. 1(a), dashed red arrow). Moreover, earlier experiments (at 217 nm) suggest that a large fraction of these H-atoms with low TKER occur as a result of C–H bond dissociation in hot S_0 molecules, rather than N–H bond cleavage.[26] These earlier observations directly concur with our findings presented in Fig. 6(a) and 6(b): upon selectively deuterating at the N–H site we almost exclusively observe low TKER H-atoms eliminated through C–H bond dissociation. Guided by all of these previous works, we therefore propose that $\tau_{stat} = 1.0 \pm 0.4$ ns correlates to the timescale for statistical unimolecular C–H bond dissociation from vibrationally hot S_0 molecules.

As alluded to above, the statistical C–H fission dynamics from hot S_0 species have not terminated by the temporal limit of our experiments ($\Delta t = 1.2$ ns). We thus suggest that the value for τ_{stat} extracted from the kinetic fit to the low TKER H^+ signal transient in Fig. 6(d) should be regarded as a conservative 'lower-limit' for the timescale of such a process (*i.e.* $\tau_{stat} \geq 1$ ns). Such a consideration is also guided by previous TKER spectra reported in previous frequency-resolved experiments,[27,28] recorded at much longer time-delays of $\Delta t \sim 5$ to 10 ns. In particular, the TKER spectra recorded at 210.7 and 193 nm by Cronin *et al.*[27] ($\Delta t \sim 5$ ns) clearly possess a signal component at low TKER which has a significantly greater amplitude than the high TKER signal. In line with our above comments, this further suggests that by 1.2 ns, statistical H-atom elimination dynamics from hot S_0 are not complete in pyrrole. Based on our current measurements, it is unclear whether or not this additional signal rise after 5 ns comes about solely through C–H fission from S_0. It may be possible that analogous statistical N–H bond fission from hot S_0 species will take longer than C–H fission, and begin to contribute to the large low TKER signal observed by Cronin *et al.*[27] and Rubio-Lago *et al.*[28] by $\Delta t = 5$–10 ns.

To close this section, we briefly consider the notable contribution of statistical H-atom elimination dynamics after populating $^1\pi\pi^*$ ($^1B_2$) at 200 nm, relative to the apparently negligible participation of this behaviour (by 1.2 ns) following direct excitation to $1^1\pi\sigma^*$ ($^1A_2$) at 250 and 238 nm. Whilst we cannot provide a definitive answer to this observation, we postulate that, unlike direct excitation to $1^1\pi\sigma^*$ ($^1A_2$) where S_0 can only be populated *via* IC from $1^1\pi\sigma^*$ ($^1A_2$) $\rightarrow$ S_0, excitation to $^1\pi\pi^*$ ($^1B_2$) offers a number of possible pathways through which S_0 can be re-populated: for example, direct IC from $^1\pi\pi^*$ ($^1B_2$) $\rightarrow$ S_0 mediated by

appropriate CIs as well as sequential IC from $^1\pi\pi^*$ ($^1B_2$) $\rightarrow$ $1^1\pi\sigma^*$ ($^1A_2$) $\rightarrow$ S_0. Coupled to the increased internal energy following excitation to $^1\pi\pi^*$ ($^1B_2$), this may enable access to higher energy dissociation channels from hot S_0 species, such as C–H fission, potentially rationalising the notable difference in statistical H-atom elimination dynamics at the excitation wavelengths studied here.

4 Conclusions

Using a combination of ultrafast time-resolved ion-yield and time-resolved velocity map ion imaging techniques we have directly probed H-atom elimination dynamics in pyrrole following: (*i*) direct excitation to the $1^1\pi\sigma^*$ ($^1A_2$) state at both 250 and 238 nm; and (*ii*) initial photoexcitation to the higher energy $^1\pi\pi^*$ ($^1B_2$) state at 200 nm.

After direct excitation to the dissociative $1^1\pi\sigma^*$ ($^1A_2$) surface we almost exclusively observe H-atoms born with large amounts of kinetic energy release (6500–7200 cm^{-1}), which are attributed to rapid dissociation of the N–H bond and the formation of $C_4H_4N(\tilde{X})$ + H photoproducts. At 250 nm, we measure an ultrafast appearance time of 126 $\pm$ 28 fs for these high kinetic energy H-atoms. With the aid of complementary measurements of D-atom elimination from pyrrole-d_1 molecules, we conclude that excitation at 250 nm imparts population into the quasi-bound 3s Rydberg well of the $1^1\pi\sigma^*$ ($^1A_2$) surface in the vertical Franck–Condon region, which then rapidly tunnels through a small exit barrier (>630 cm^{-1}), subsequently leading to ultrafast N–H bond fission. At 238 nm, excitation to $1^1\pi\sigma^*$ ($^1A_2$) occurs above the exit barrier to dissociation, leading to extremely rapid N–H bond fission within 46 $\pm$ 22 fs. Measurements on pyrrole-d_1 indicate that tunnelling plays a negligible role in the N–H bond cleavage dynamics at 238 nm.

Excitation at a wavelength of 200 nm initially accesses the higher lying $^1\pi\pi^*$ ($^1B_2$) state, which yields a bi-modal distribution of H-atoms with high amounts of kinetic energy as well as low kinetic energies (with a 'statistical' profile), in contrast to the measurements at 250 and 238 nm. The H-atoms possessing large amounts of kinetic energy are once again attributed to the formation of $C_4H_4N(\tilde{X})$ + H photoproducts, except this time generated though a sequential $^1\pi\pi^*$ ($^1B_2$) $\rightarrow$ $1^1\pi\sigma^*$ ($^1A_2$) $\rightarrow$ N–H fission mechanism. We extract an appearance time-constant of 52 $\pm$ 12 fs for H-atoms formed *via* this process. Based on this timescale, this implies that the initial $^1\pi\pi^*$ ($^1B_2$) $\rightarrow$ $1^1\pi\sigma^*$ ($^1A_2$) internal conversion step (*via* a $^1\pi\pi^*/1^1\pi\sigma^*$ CI located along a ring-deformation coordinate[30–33]) takes place on a sub-50 fs timeframe, which is in good accord with findings from previous complementary experimental[23] and theoretical work.[32,33]

The appearance of low kinetic energy H-atoms at 200 nm is characterised by a bi-exponential rise, with associated time-constants of 108 $\pm$ 20 fs and 1.0 $\pm$ 0.4 ns. The former ultrafast time-constant of 108 $\pm$ 20 fs is attributed to H-atoms formed through undesired multiphoton processes. However, the latter slower rise in low kinetic energy H-atom signal is assigned to the onset of statistical unimolecular H-atom elimination from vibrationally hot S_0 ground state species, after initial recoupling onto S_0 through appropriate CIs (*e.g.* $1^1\pi\sigma^*/S_0$ or $^1\pi\pi^*/S_0$ CIs). Specifically, probing D-atom elimination from pyrrole-d_1 at 200 nm reveals that, up to 1.2 ns after excitation, statistical H-atom elimination only results from C–H bond cleavage on S_0. Moreover, based on our measurements here and by comparison

with earlier frequency-domain studies,[27,28] these statistical C–H fission dynamics appear to be incomplete by 1.2 ns, indicating that the extracted time-constant of ~1.0 ns should be considered as a 'lower-limit' for the timescale of such a process in pyrrole.

More generally, the ultrafast time-resolved studies presented here provide new and complementary insights into the dynamical processes which occur following photoexcitation of pyrrole between 250 to 200 nm. In particular, these studies for the first time highlight: (*i*) the role of tunnelling after direct excitation to the $1^1\pi\sigma^*$ ($^1A_2$) surface at 250 nm, providing strong evidence that this state does indeed possess a quasi-bound 3s Rydberg well in the vertical Franck–Condon region (similar to $^1n\sigma^*$ and $^1\pi\sigma^*$ surfaces in other related species, such as ammonia[57] and aniline,[56] respectively); and (*ii*) the onset of slower statistical C–H bond fission after (re-)coupling onto a vibrationally hot S_0 ground state following initial excitation to $^1\pi\pi^*$ ($^1B_2$), and the timescales on which this behaviour starts to occurs.

Acknowledgements

The authors gratefully thank Dr Dave Hadden and Dr Michael Staniforth for experimental assistance and helpful discussions and Professor Mike Ashfold for helpful discussions. G.M.R. and A.S.C. thank the Leverhulme Trust for a post-doctoral research fellowship and doctoral funding, respectively. C.A.W. thanks the EPSRC for a doctoral research fellowship. J.D.Y. thanks the University of Warwick for a doctoral training award. H.Y. thanks the NSF for a graduate research assistantship. S.U. and V.G.S. would like to thank the NSF and EPSRC for grants (NSF-CHE-0924456 and EP/H003401) which have been awarded through the International Collaboration in Chemistry Program. V.G.S. would also like to thank the Royal Society for a University Research Fellowship.

References

1 A. L. Sobolewski, W. Domcke, C. Dedonder-Lardeux and C. Jouvet, *Phys. Chem. Chem. Phys.*, 2002, **4**, 1093–1100.
2 M. N. R. Ashfold, B. Cronin, A. L. Devine, R. N. Dixon and M. G. D. Nix, *Science*, 2006, **312**, 1637–1640.
3 M. N. R. Ashfold, G. A. King, D. Murdock, M. G. D. Nix, T. A. A. Oliver and A. G. Sage, *Phys. Chem. Chem. Phys.*, 2010, **12**, 1218–1238.
4 N. L. Evans and S. Ullrich, *J. Phys. Chem. A*, 2010, **114**, 11225–11230.
5 M. G. D. Nix, A. L. Devine, B. Cronin and M. N. R. Ashfold, *J. Chem. Phys.*, 2007, **126**, 124312.
6 K. L. Wells, D. J. Hadden, M. G. D. Nix and V. G. Stavros, *J. Phys. Chem. Lett.*, 2010, **1**, 993–996.
7 S. Ullrich, T. Schultz, M. Z. Zgierski and A. Stolow, *Phys. Chem. Chem. Phys.*, 2004, **6**, 2796–2801.
8 C. T. Middleton, K. de La Harpe, C. Su, Y. K. Law, C. E. Crespo-Hernandez and B. Kohler, *Annu. Rev. Phys. Chem.*, 2009, **60**, 217–239.
9 H. Satzger, D. Townsend, M. Z. Zgierski, S. Patchkovskii, S. Ullrich and A. Stolow, *Proc. Natl. Acad. Sci. U. S. A.*, 2006, **103**, 10196–10201.
10 A. Iqbal and V. G. Stavros, *J. Phys. Chem. Lett.*, 2010, **1**, 2274–2278.
11 G. M. Roberts, C. A. Williams, M. J. Paterson, S. Ullrich and V. G. Stavros, *Chem. Sci.*, 2012, **3**, 1192–1199.
12 A. L. Devine, B. Cronin, M. G. D. Nix and M. N. R. Ashfold, *J. Chem. Phys.*, 2006, **125**, 184302.
13 R. Montero, A. P. Conde, V. Ovejas, F. Castano and A. Longarte, *J. Phys. Chem. A*, 2012, **116**, 2698–2703.

14 A. Iqbal and V. G. Stavros, *J. Phys. Chem. A*, 2010, **114**, 68–72.
15 G. M. Roberts, A. S. Chatterley, J. D. Young and V. G. Stavros, *J. Phys. Chem. Lett.*, 2012, **3**, 348–352.
16 M. N. R. Ashfold, A. L. Devine, R. N. Dixon, G. A. King, M. G. D. Nix and T. A. A. Oliver, *Proc. Natl. Acad. Sci. U. S. A.*, 2008, **105**, 12701–12706.
17 M. G. D. Nix, A. L. Devine, B. Cronin and M. N. R. Ashfold, *Phys. Chem. Chem. Phys.*, 2006, **8**, 2610–2618.
18 Y. Zhang, T. A. A. Oliver, M. N. R. Ashfold and S. E. Bradforth, *Faraday Discuss.*, 2012, **157**, 141–163.
19 T. A. A. Oliver, Y. Zhang, M. N. R. Ashfold and S. E. Bradforth, *Faraday Discuss.*, 2011, **150**, 439–458.
20 F. F. Crim, *Faraday Discuss.*, 2012, **157**, 9–26.
21 D. Murdock, S. J. Harris, T. N. V. Karsili, G. M. Greetham, I. P. Clark, M. Towrie, A. J. Orr-Ewing and M. N. R. Ashfold, *J. Phys. Chem. Lett.*, 2012, **3**, 3715–3720.
22 H. Lippert, H. H. Ritze, I. V. Hertel and W. Radloff, *ChemPhysChem*, 2004, **5**, 1423–1427.
23 R. Montero, A. P. Conde, V. Ovejas, M. Fernandez-Fernandez, F. Castano, J. R. V. de Aldana and A. Longarte, *J. Chem. Phys.*, 2012, **137**, 064317.
24 D. A. Blank, S. W. North and Y. T. Lee, *Chem. Phys.*, 1994, **187**, 35–47.
25 J. Wei, A. Kuczmann, J. Riedel, F. Renth and F. Temps, *Phys. Chem. Chem. Phys.*, 2003, **5**, 315–320.
26 J. Wei, J. Riedel, A. Kuczmann, F. Renth and F. Temps, *Faraday Discuss.*, 2004, **127**, 267–282.
27 B. Cronin, M. G. D. Nix, R. H. Qadiri and M. N. R. Ashfold, *Phys. Chem. Chem. Phys.*, 2004, **6**, 5031–5041.
28 L. Rubio-Lago, D. Zaouris, Y. Sakellariou, D. Sofikitis, T. N. Kitsopoulos, F. Wang, X. Yang, B. Cronin, A. L. Devine, G. A. King, M. G. D. Nix, M. N. R. Ashfold and S. S. Xantheas, *J. Chem. Phys.*, 2007, **127**, 064306.
29 V. Vallet, Z. G. Lan, S. Mahapatra, A. L. Sobolewski and W. Domcke, *J. Chem. Phys.*, 2005, **123**, 144307.
30 M. Barbatti, M. Vazdar, A. J. A. Aquino, M. Eckert-Maksic and H. Lischka, *J. Chem. Phys.*, 2006, **125**, 164323.
31 B. Sellner, M. Barbatti and H. Lischka, *J. Chem. Phys.*, 2009, **131**, 024312.
32 M. Vazdar, M. Eckert-Maksic, M. Barbatti and H. Lischka, *Mol. Phys.*, 2009, **107**, 845–854.
33 M. Barbatti, J. Pittner, M. Pederzoli, U. Werner, R. Mitric, V. Bonacic-Koutecky and H. Lischka, *Chem. Phys.*, 2010, **375**, 26–34.
34 H. Nakatsuji, O. Kitao and T. Yonezawa, *J. Chem. Phys.*, 1985, **83**, 723–734.
35 H. Nakano, T. Tsuneda, T. Hashimoto and K. Hirao, *J. Chem. Phys.*, 1996, **104**, 2312–2320.
36 M. H. Palmer, I. C. Walker and M. F. Guest, *Chem. Phys.*, 1998, **238**, 179–199.
37 O. Christiansen, J. Gauss, J. F. Stanton and P. Jorgensen, *J. Chem. Phys.*, 1999, **111**, 525–537.
38 J. Wan, J. Meller, M. Hada, M. Ehara and H. Nakatsuji, *J. Chem. Phys.*, 2000, **113**, 7853–7866.
39 B. O. Roos, P. A. Malmqvist, V. Molina, L. Serrano-Andres and M. Merchan, *J. Chem. Phys.*, 2002, **116**, 7526–7536.
40 G. M. Roberts and V. G. Stavros, in *Ultrafast Phenomena in Molecular Sciences*, ed. L. Banares, Springer, in press.
41 K. L. Wells, G. Perriam and V. G. Stavros, *J. Chem. Phys.*, 2009, **130**, 074304.
42 G. M. Roberts, C. A. Williams, J. D. Young, S. Ullrich, M. J. Paterson and V. G. Stavros, *J. Am. Chem. Soc.*, 2012, **134**, 12578–12589.
43 A. T. J. B. Eppink and D. H. Parker, *Rev. Sci. Instrum.*, 1997, **68**, 3477–3484.
44 U. Even, J. Jortner, D. Noy, N. Lavie and C. Cossart-Magos, *J. Chem. Phys.*, 2000, **112**, 8068–8071.
45 G. M. Roberts, J. L. Nixon, J. Lecointre, E. Wrede and J. R. R. Verlet, *Rev. Sci. Instrum.*, 2009, **80**, 053104.
46 P. M. Regan, S. R. Langford, A. J. Orr-Ewing and M. N. R. Ashfold, *J. Chem. Phys.*, 1999, **110**, 281–288.
47 A. Iqbal, L. J. Pegg and V. G. Stavros, *J. Phys. Chem. A*, 2008, **112**, 9531–9534.
48 Below $\sim$7000 cm^{-1} we note that the VMI spectrometer has a restricted resolution of $\Delta E/E \sim 15$–20%.
49 A. J. Gianola, T. Ichino, R. L. Hoenigman, S. Kato, V. M. Bierbaum and W. C. Lineberger, *J. Phys. Chem. A*, 2004, **108**, 10326–10335.
50 P. L. Houston, in *Imaging in Molecular Dynamics: Technology and Applications*, ed. B. J. Whitaker, Cambridge University Press, Cambridge, 2003, ch. 1, pp. 3–19.
51 C. A. Williams, G. M. Roberts, H. Yu, N. L. Evans, S. Ullrich and V. G. Stavros, *J. Phys. Chem. A*, 2012, **116**, 2600–2609.

52 D. J. Hadden, C. A. Williams, G. M. Roberts and V. G. Stavros, *Phys. Chem. Chem. Phys.*, 2011, **13**, 4494–4499.
53 D. J. Hadden, K. L. Wells, G. M. Roberts, L. T. Bergendahl, M. J. Paterson and V. G. Stavros, *Phys. Chem. Chem. Phys.*, 2011, **13**, 10342–10349.
54 A. Iqbal, M. S. Y. Cheung, M. G. D. Nix and V. G. Stavros, *J. Phys. Chem. A*, 2009, **113**, 8157–8163.
55 H. Reisler and A. I. Krylov, *Int. Rev. Phys. Chem.*, 2009, **28**, 267–308.
56 G. A. King, T. A. A. Oliver and M. N. R. Ashfold, *J. Chem. Phys.*, 2010, **132**, 214307.
57 M. N. R. Ashfold, R. N. Dixon, M. Kono, D. H. Mordaunt and C. L. Reed, *Philos. Trans. R. Soc. London, Ser. A*, 1997, **355**, 1659–1674.
58 G. A. King, T. A. A. Oliver, M. G. D. Nix and M. N. R. Ashfold, *J. Chem. Phys.*, 2010, **132**, 064305.
59 At 200 nm we acknowledge that the 'low TKER' and 'high TKER' signal components in the TKER spectra in Fig. 6(a) are partially convoluted. This may, in principle, also provide an alternative explanation for the 'effective' non-limiting β_2 value extracted for the 'high TKER' feature between 6000–10000 cm^{-1}, given the near-isotropic distribution of the underlying 'low TKER' signal component ($\beta_2 \approx 0$); this explanation was previously adopted by Wei *et al.* at 217 nm (see ref. 26). A fit to the profile of the TKER spectrum at $\Delta t = 1.2$ ns (Fig. S3) indicates that the low TKER feature only contributes ~7% of the total signal between 6000–10000 cm^{-1}, which would in turn result in a 'corrected' β_2 value of −0.54 (see ref. 26). As such, we favour the arguments put forward in the main text (section 3.2a) to explain the non-limiting value of $\beta_2 \approx -0.5$ for the high TKER feature at 200 nm.
60 B. Cronin, A. L. Devine, M. G. D. Nix and M. N. R. Ashfold, *Phys. Chem. Chem. Phys.*, 2006, **8**, 3440–3445.
61 This is a conservative estimate based on the value given in ref. 60, which corresponds to the fully deuterated pyrrole, *i.e.*, pyrrole-d_5.

